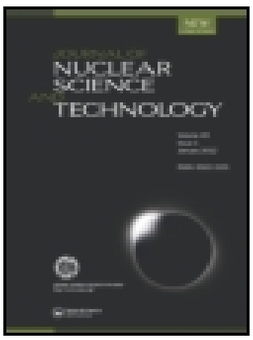

Journal of Nuclear Science and Technology

ISSN: 0022-3131 (Print) 1881-1248 (Online) Journal homepage: http://www.tandfonline.com/loi/tnst20

Numerical solutions for the kinematic model of pebble flow velocity profiles and its applications in pebble-bed nuclear reactor

Yu-shi Tang, Li-guo Zhang, Qiu-ju Guo, Jian-zhu Cao & Jie-juan Tong

To cite this article: Yu-shi Tang, Li-guo Zhang, Qiu-ju Guo, Jian-zhu Cao & Jie-juan Tong (2017): Numerical solutions for the kinematic model of pebble flow velocity profiles and its applications in pebble-bed nuclear reactor, Journal of Nuclear Science and Technology, DOI: 10.1080/00223131.2017.1331763

To link to this article: http://dx.doi.org/10.1080/00223131.2017.1331763

JOURNAL OF NUCLEAR SCIENCE AND TECHNOLOGY, 2017
https://doi.org/10.1080/00223131.2017.1331763

ARTICLE

Numerical solutions for the kinematic model of pebble flow velocity profiles and its applications in pebble-bed nuclear reactor

Yu-shi Tang[a], Li-guo Zhang[b], Qiu-ju Guo[a], Jian-zhu Cao[b] and Jie-juan Tong[b]

[a]State Key Laboratory of Nuclear Physics and Technology, School of Physics, Peking University, Beijing, P. R. China; [b]Institute of Nuclear and New Energy Technology, Collaborative Innovation Center of Advanced Nuclear Energy Technology, Key Laboratory of Advanced Reactor Engineering and Safety of Ministry of Education, Tsinghua University, Beijing, P. R. China

ABSTRACT

The modular pebble-bed nuclear reactor (PBR) is a candidate Generation IV reactor being developed. The pebble flow in the very slow draining of fuel pebbles draws attention for its implications on core physical design and reactor physics analysis. One of the effective and simplified methods to address this problem is the kinematic model which is based on continuous theory to derive a diffusion equation for vertical velocity. This paper investigates the appropriate numerical solutions for the kinematic model of pebble flow velocity profiles in PBR geometry. Our method is based on a previously proposed transformed Cartesian coordinates and uses the implicit Crank–Nicholson integration scheme with two different treatments of the boundary conditions. Validations show that this numerical solution gives preferable agreements with the experimental results in the reference. Finally, the simulated velocity profiles are applied in the investigation of two pebble burnup-related issues, which are the pebble residence time prediction and the channel scheme in realistic high-temperature reactor pebble-bed modules reactor core geometry.

ARTICLE HISTORY
Received 24 January 2017
Accepted 16 May 2017

KEYWORDS
Burnup calculation; HTGR; numerical simulation

1. Introduction

The high temperature gas-cooled nuclear reactor (HTR) is a candidate Generation IV reactor being developed as one of the most economical, fuel-efficient, and the safest nuclear powers [1]. In China, large interest has been initiated on modular pebble-bed HTR, in which the notable uranium-based graphite fuel pebbles have been introduced. Researches have been focused on the high-temperature reactor pebble-bed modules (HTR-PM) being developed by Tsinghua University [2]. The continuous refueling process of fuel pebbles without shutdown during operation is a major advantage of pebble-bed nuclear reactor (PBR) over other core designs. In this process, fuel pebbles are introduced from the top and drain very slowly in the reactor core, which is typically in the shape of an upper cylindrical vessel, a bottom funnel and an exit pipe (Figure 1). It is important to have a clear understanding of the flow profile of fuel pebbles in PBR for its implications on reactor physical design, such as the geometry dependence of the mean streamlines and the wall effects [3]. Furthermore, the pebble flow profile is an essential input in the reliable prediction of reactor physics characteristics such as the fuel burnup, namely the depletion of the fuel in pebbles. The subsequent purpose of this research on pebble flow is to generate the burnup distribution of fuel pebbles, which has been revealed to be essentially relevant to issues in reactor safety as well as economic efficiency in our previous research [4].

The pebble flow research in a realistic dynamic PBR core, originated from dense slow granular flow study in silos and hoppers [5], have been mostly investigated with experiments focused on static packing of spheres and particle tracking [6]. However, it is necessary to further study the pebble flow with numerical approaches, considering the limited information obtained from experiment and the complexity of dense slow pebble flow in PBR. The discrete element method (DEM) and the kinematic model are the two representative methods to numerically predict the profiles of dense slow pebble flow [3]. The DEM addresses the dynamics of the system at the micro-contact level with establishments of pebble contact model and motion equations, while it is fairly complicated due to the large parameter space and some unmeasurable contact parameters [7,8]. The kinematic model ignores the stress field and attempts a macroscopic continuous diffusion theory of the bulk only with a simplified diffusion equation, and it is simple to use and applicable in various geometries of dense slow [5,9]. Although DEM has been used in coupled pebble flow and coolant flow model to predict PBR core physics [10], the kinematic model has also drawn attention for its simplicity and satisfactory results in flow velocity profiles simulation. Hence, this paper makes use of the kinematic model for pebble velocity profiles in PBR.

To address this problem numerically, previous numerical solutions to the kinematic model have been

CONTACT Li-guo Zhang lgzhang@tsinghua.edu.cn

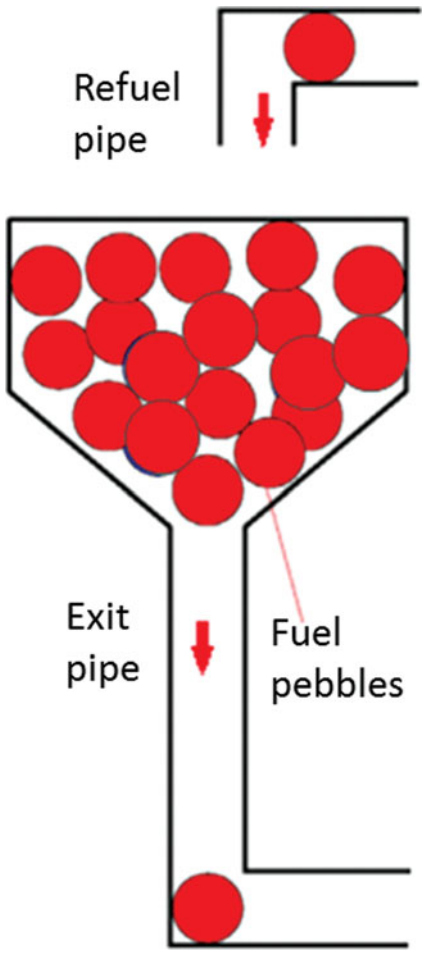

Figure 1. The schematic diagram of a PBR core geometry.

studied, advanced and subsequently validated as appropriate in PBR geometry. Furthermore, velocity profiles derived by the numerical solutions have been applied to investigate pebble burnup-related issues in realistic HTR-PM geometry. So this paper is organized as follows. The next section of this paper introduces the kinematic model and the boundary conditions of PBR core geometry. Then, the subsequent section introduces a numerical solution adopting a transformed Cartesian coordinates previously proposed in [3], and illustrates the discretizations for the diffusion equation with two boundary treatment schemes. Subsequently, the numerical solutions in PBR geometry are validated as appropriate in PBR geometry by comparing the simulated results with published experimental results. Later, with the obtained velocity profiles, we investigate two burnup-related applications which are the pebble residence time prediction and the channel scheme in realistic HTR-PM geometry. The last section is conclusions and discussion.

2. Kinematic model of pebble flow

2.1. The kinematic model

The research of pebble flow was initially enlightened by the study of dense slow granular flow in silos and hoppers. Nedderman and Tüzün derived a continuum equation from the constitutive law (Equation (1)) and the incompressibility condition, and the continuum diffusion equation for vertical velocity was given as Equation (2) for dense slow granular flow in a quasi-two-dimensional silo [9]:

$$V_x = -B\nabla_\perp V_z, \tag{1}$$

$$\frac{\partial V_z}{\partial z} = B\nabla_\perp^2 V_z, \tag{2}$$

where $\nabla_\perp^2$ is the horizontal Laplacian, the kinematic constant B refers to the 'diffusion length,' as it has the unit of length. The value of B which indicates the granule-diffusing ability was thought to be related with granule material [11,12].

By enforcing that velocity at the side wall must be tangential to the wall, Equation (3) can be obtained as boundary condition at side wall, where K is the cotangent value of slope angle (exterior wall angle, which is 30°in Figure 1) in the cone region. Boundary condition for V_x at side wall can then be derived from V_z as Equation (4).

$$\left.\frac{\partial V_z}{\partial x}\right|_{x=R} = -\frac{KV_z}{B}, \tag{3}$$

$$V_x|_{x=R} = KV_z. \tag{4}$$

2.2. Numerical discretization of the diffusion equation

By considering the horizontal Laplacian in the diffusion equation (Equation (2)) and the axial symmetry of the PBR core geometry, V_z can be seen as a function of r. The diffusion equation in cylindrical coordinates can be given as

$$\frac{\partial V_z}{\partial z} = B\frac{\partial^2 V_z}{\partial r^2} + B\frac{1}{r}\frac{\partial V_z}{\partial r}. \tag{5}$$

To numerically solve the partial differential equation in the cylinder is straightforward, since we can make use of the rectangular grid, whereas the radius R of the reactor core in cone region is the function of z, so a better numerical method originally proposed in [3] is used in this study. The Cartesian coordinates which is transformed from the cylindrical coordinates, let $\alpha = r/R(z)$, $\gamma = z$, is adopted. This allows solving the equation over the range $0 < \alpha < 1$ independent of variable R. Diffusion equation in the Cartesian coordinates can then be derived as

$$\frac{\partial V_\gamma}{\partial \gamma} = \frac{B}{R^2}\frac{\partial^2 V_\gamma}{\partial \alpha^2} + \left(\frac{B}{\alpha R^2} + \frac{\alpha K}{R}\right)\frac{\partial V_\gamma}{\partial \alpha}. \tag{6}$$

A mesh strategy is adopted to numerically solve Equation (6) in a half-size PBR geometry (divided by

central axis). This quasi-two-dimensional α–γ simulation domain is meshed with grid points of $(N + 1)$ columns and $(M + 1)$ rows. Let $V_j^i = V(j\Delta\alpha, i\Delta\gamma)$ be the vertical velocity at grid point (j, i), $j = 0,1,\ldots, N$ (from center to the side walls), $i = 0,1,\ldots, M$ (from bottom to top of the core), where$N = \Delta\alpha^{-1}$, $M = H/\Delta\gamma$ (H is the height of the core). With the Crank–Nicholson integration scheme (or implicit central difference scheme) applied to Equation (6), the diffusion equation can be approximated as Equation (7)

$$\frac{V_j^{i+1} - V_j^i}{\Delta\gamma} = \frac{B}{2\Delta\alpha^2 R^2}\left(V_{j+1}^{i+1} - 2V_j^{i+1} + V_{j-1}^{i+1} + V_{j+1}^i - 2V_j^i + V_{j-1}^i\right) + \left(\frac{B}{4j\Delta\alpha^2 R^2} + \frac{jK}{4R}\right) \times \left(V_{j+1}^{i+1} - V_{j-1}^{i+1} + V_{j+1}^i - V_{j-1}^i\right), \quad (7)$$

where all R and K are evaluated at $\gamma = \Delta\gamma(i + 1/2)$. It also indicates that the vertical velocity profiles of lower points at ith row contribute to the vertical velocity of points at the $(i + 1)$th row.

Similarly Equation (1) can be numerically integrated from $z = 0$ using the central difference scheme to obtain the horizontal velocity field (let V_x be written as u in discretization):

$$u_j^i = -\frac{B}{2\Delta\alpha R}\left(V_{j+1}^i - V_{j-1}^i\right). \quad (8)$$

2.3. Numerical discretization of boundary conditions

In a half-size PBR geometry divided by central axis, boundary condition for vertical velocity at $\alpha = 0$ (central axis of the core) is set as Equation (9) to ensure the differentiability.

$$\left.\frac{\partial V_z}{\partial\alpha}\right|_{\alpha=0} = 0. \quad (9)$$

Boundary condition at $\alpha = 1$ (side walls) for vertical velocity in the Cartesian coordinates is given as Equation (10) according to Equation (3).

$$\left.\frac{\partial V_z}{\partial\alpha}\right|_{\alpha=1} = -\frac{KV_zR}{B}. \quad (10)$$

To numerically solve the problem, two boundary conditions are introduced for vertical velocity in the following part.

2.3.1. Forward or backward difference scheme

The first one is our originally proposed second-order accurate forward or backward difference scheme. The second-order accurate forward difference scheme of Equation (9) at $j = 0$ is derived as

$$\frac{-V_2^{i+1} + 4V_1^{i+1} - 3V_0^{i+1}}{2\Delta\alpha} = 0, \quad (11)$$

while for $j = N$, the second-order accurate backward difference scheme of Equation (10) is

$$\frac{3V_N^{i+1} - 4V_{N-1}^{i+1} + V_{N-2}^{i+1}}{2\Delta\alpha} = -\frac{KV_N^{i+1}R(\beta)}{B}. \quad (12)$$

2.3.2. Central difference scheme

The second one is the central difference scheme [3]. First, Equations (13) and (14) can be generated when we apply the second-order accurate central difference scheme on Equations (9) and (10).

$$\frac{V_1^i - V_{-1}^i}{2\Delta\alpha} = 0, \quad (13)$$

$$\frac{V_{N+1}^i - V_{N-1}^i}{2\Delta\alpha} = -\frac{KV_N^iR}{B}. \quad (14)$$

When $j = 0$ is set in Equation (7), and by reference to Equation (13), boundary condition at $\alpha = 0$ can be derived as

$$\frac{V_0^{i+1} - V_0^i}{\Delta\gamma} = \frac{B}{\Delta\alpha^2 R^2}\left(V_1^{i+1} - V_0^{i+1} + V_1^i - V_0^i\right). \quad (15)$$

When $j = N$ in Equation (7), and by reference to Equation (14), boundary condition at $\alpha = 1$ is obtained as Equation (16).

$$\frac{V_N^{i+1} - V_N^i}{\Delta\gamma} = \frac{B}{\Delta\alpha^2 R^2}\left(V_{N-1}^{i+1} - V_N^{i+1} + V_{N-1}^i - V_N^i\right) - \left(\frac{(2N+1)K}{2R} + \frac{K^2}{2B}\right)\left(V_N^{i+1} + V_N^i\right), \quad (16)$$

whereas without any special treatments to the boundary conditions for horizontal velocity (Equation (4)), $u_0^i = 0$ and $u_N^i = KV_N^i$ can be simply generated at $j = 0$ and $j = N$, respectively.

3. Implementations and validations

Let $\mathbf{V^i} = (V_0^i, V_1^i, \ldots, V_N^i)^T$ be the vertical velocity vector for grid points in row i, then the above numerical scheme can be written in the form $\mathbf{AV^{i+1}} = \mathbf{YV^i}$, where $\boldsymbol{A}$ and $\boldsymbol{Y}$ are tridiagonal matrices. This system can be efficiently solved by recursion of M times. The above scheme is implemented with Matlab (Version: R2014a) to solve the matrix equation. Since $\boldsymbol{A}$ is a tridiagonal matrix, the method of forward elimination and backward substitution (or the chasing method) is recommended to solve the matrix equation [13].

The following part will present and compare the pebble velocity profiles from the two treatments of boundary conditions for vertical velocity mentioned previously. Validations of the results are performed by comparing the simulated results with experimental results given in reference [5] for certain hopper geometries, which are the same as PBR geometry except for the elimination of the lower exit pipe. The orifice size

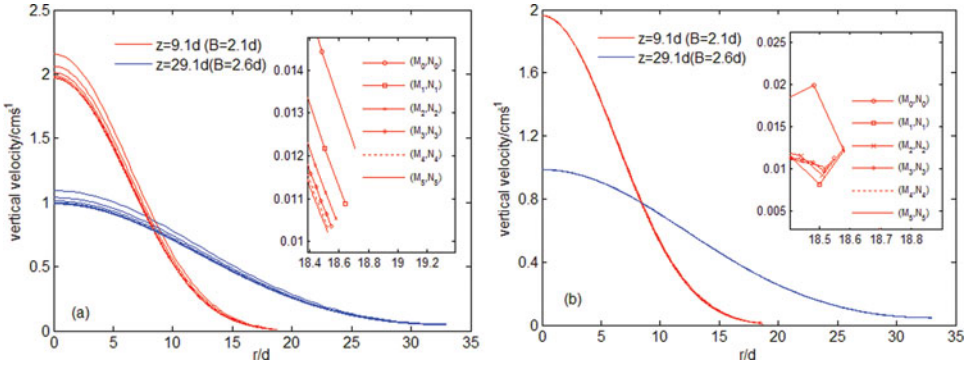

Figure 2. The variation of absolute vertical velocity profiles derived with (a) Method 1 and (b) Method 2 under different grid schemes at two heights (9.1*d* and 29.1*d*) for slope angled at 30° in geometry.

(R_o = 9 mm) and the radius of the upper cylinder (R_u = 100 mm) are fixed while the slope angle is varied to $\theta = 30°, 45°, 60°$. Velocity profiles at two heights, 9.1*d* and 29.1*d* (*d* is the pebble diameter, 3 mm) are given for each geometry in the reference. Since the initial velocity at $z = 0$ (the bottom of the funnel) is not given, the relative vertical velocity (vertical velocity normalized by the maximum vertical velocity at a given height) is calculated and used in the comparisons (see Figure 4). Besides, the experimental results in [5] are generated under a quasi-two-dimensional silo, which would generate an expanding and discretization of the diffusion equation different from the three-dimensional one we introduced before. Therefore, the two-dimensional transforms are used in the following validation; however, it would not be given here in detail since it is almost the same as the one introduced in Section 2.2 except for slight differences in the coefficients of the equations.

To compare the pebble velocity profiles in Cartesian coordinates from the two treatments of boundary conditions, the two boundary treatments are used respectively with the implicit Crank–Nicholson integration scheme of diffusion equation in the Cartesian coordinates in PBR geometry. Here we denote the forward or backward difference treatment as Method 1 and the central difference treatment as Method 2.

Before comparison, the grid dependence of the velocity profiles with the two methods is tested. The velocity profiles in each geometry of these two methods are generated using different grid schemes (the initial velocity at the orifice was set as 5 cm/s). We have compared the velocity profiles from six different grid schemes, which could be notified as (M_0,N_0), (M_1,N_1) …(M_5,N_5), where *M* and *N* are the number of the vertical and the horizontal grid points. (M_0,N_0) is the initial grid scheme which has the least number of grid points, then the number of grid points in the subsequent grid scheme is set to be doubled. Therefore, $M_0/M_1 = \cdots = M_4/M_5 = 1/2$; $N_0/N_1 = \cdots = N_4/N_5 = 1/2$, which also indicates $\Delta\gamma_0 = 2\Delta\gamma_1 = \cdots = 32\Delta\gamma_5$ and $\Delta\alpha_0 = 2\Delta\alpha_1 = \cdots = 32\Delta\alpha_5$. For instance, the horizontal and vertical grid intervals under the 30° geometry are set as dr = d/2, $dz = \sqrt{3}\ dr$ in the initial grid scheme, in which the number of grids are 66 and 346 in the horizontal and vertical directions. The numbers of horizontal and vertical grids in the last scheme (M_5,N_5) are 2112 and 11,072, which correspond to $dr = d/64$, $dz = \sqrt{3}\ dr/32$. Figure 2 shows the variation of absolute vertical velocity profiles derived under different grid schemes with Method 1 and Method 2 in 30° geometry. Figure 3 gives the variation rate of the average vertical velocity under different grid schemes for these two methods in 30° geometry. For 45° and 60° geometries, figures and details of the grid tests on the velocity profiles are not given here since the basic tendency keeps the same as the 30° geometry. Figure 2(a) shows that the velocity profiles of Method 1 would decrease when grid number increases, and would gradually stabilize at the last (M_5,N_5) scheme. This could be seen much more clearly in the small plot in the figures, which gives the zoomed-out plot of the tails of the velocity profile at $z = 9.1d$. It could also be indicated by Figure 3(a), which reveals that the variation rate of the average vertical velocity would decrease with higher grid scheme and would finally result at a rate of less than 0.5% under the final scheme (M_5,N_5). Figure 2(b) shows that little instabilities appear in the tails of the velocity profiles generated by Method 2, especially for the velocity at $z = 9.1d$. The instability would gradually decrease with increased grid number, but it does not get fully smoothed even at the (M_5,N_5) scheme, and this is also well demonstrated by the zoomed-out plot of velocity tails at $z = 9.1$ in Figure 2(b). In general, there is no big change in the velocity profiles of Method 2 when grid number increases, which could also be reflected by the steady velocity variation rate in Figure 3(b). Due to the computing capability, higher grid scheme with grid number being 64 times of the initial grid number has not been applied here, but it could be estimated that the tendency in Figures 2 and 3 would still be the same. Besides, when comparing the stabilized velocity profile in Figure 2(a,b), it is found that the absolute value of the velocity profiles of the two methods are almost

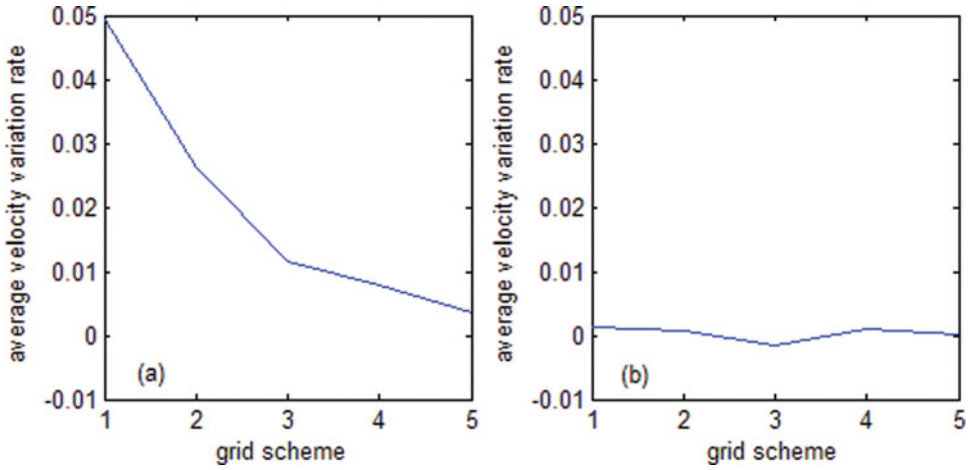

Figure 3. The variation of the decreasing rate of the average vertical velocity (at $z = 29.1d$) under different grid schemes with (a) Method 1 and (b) Method 2 for 30° geometry.

the same. This could also be verified by the overlap of the relative velocity profiles of the two methods in Figure 4.

Therefore, based on the above tests, the two methods perform differently on grid dependence. Although the results from Method 1 have a higher grid dependence regarding the velocity variation rate, it could finally stabilize at the (M_5,N_5) scheme. While Method 2 has a smaller velocity variation dependence on grid number, it would still show instabilities at the velocity tail under the (M_5,N_5) scheme. Thus, in the view of the grid dependence, Method 1 is more preferable than Method 2. However, in the real PBR application, the realistic boundary for pebble flow is actually the trajectories of the center of the boundary pebble, so there is at least a separation of a pebble radius between the realistic pebble flow boundary and the physical core boundary. Thus, the velocity profiles beyond the realistic flow boundary, where the velocity instabilities in Method 2 appear, would not make sense in the real application and could be ignored. Therefore, both the methods could be worth trying in the following validation of the simulated results with the grid scheme (M_5,N_5).

With different diffusion lengths B best fitted from corresponding experimental profiles (see legends in Figure 4), the relative velocity profiles from Method 1

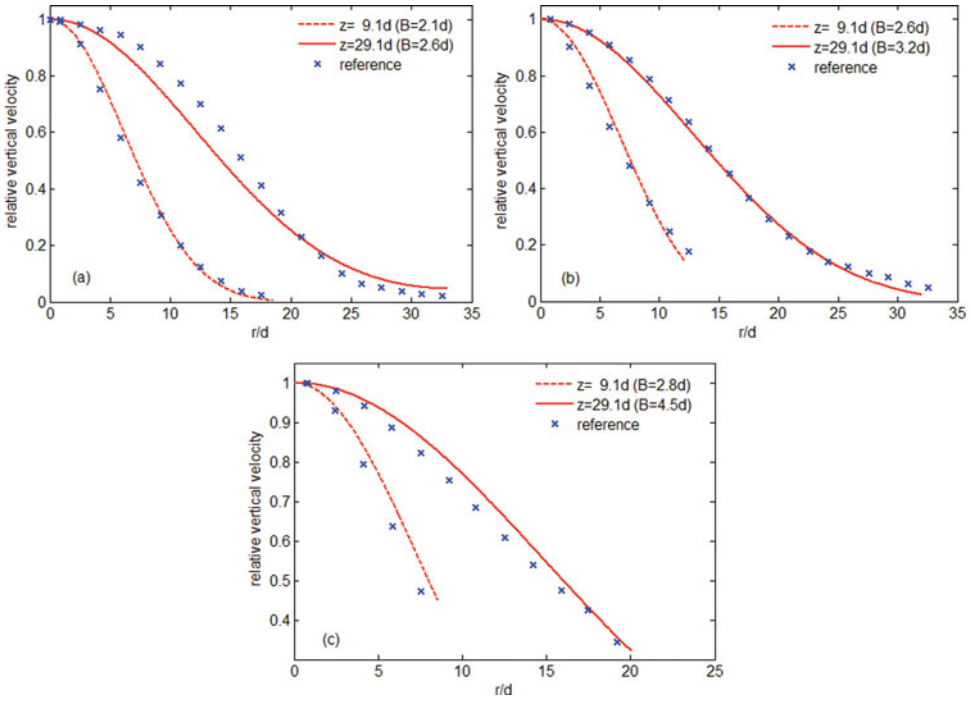

Figure 4. The relative vertical velocity profiles derived with Method 1 and Method 2 (coincide) at two heights, 9.1*d* (dotted line) and 29.1*d* (solid line), for slope angled at (a) 30°, (b) 45° and (c) 60°in reactor geometries, with comparisons to the experimental results in reference [5] (x-dotted line).

and Method 2 are obtained and compared with the experimental results in [5]. Relative profiles from the two methods are confirmed to be almost the same in core geometry, indicated by the coincidence of the relative velocity curves from the two methods.

Figure 4 also shows that the two numerical solutions predict smooth velocity profiles, free of shock-like discontinuities, quite consistent with the experiments. This reveals that the two numerical solutions give reasonable qualitative prediction of flow velocity profiles. Besides, we can see that vertical velocity is maximum at the center and declines along the increasing radius in a nearly parabolic form, showing a highly dynamic flow at the center while stagnant pebbles by the side walls. Moreover, the pebble fuel mass flow flux (here equivalent to $\int \vec{V} \cdot d\vec{S}$, where $\vec{S}$ is the directed area) at the two different heights is confirmed to be almost the same, briefly verifying the conservation of mass flow flux in the kinematic model.

In addition to the transformed Cartesian coordinates, the cylindrical coordinates is attempted in simulation as well, because cylindrical form equation matches physical geometry better and may be easily integrated into grid scheme of physics and thermal-hydraulics calculation. We find that velocity profiles derived under cylindrical coordinates demonstrate big shock-like instabilities in 45° and 60° core geometry (steeper wall slope), while it predicts velocity profiles free of shock-like discontinuities under 30° core geometry (gentler wall slope), and the results are quite consistent with the experiments. Therefore, the cylindrical coordinates may be good for the PBR 30° core geometry, but due to its poor geometry universality, it would not be discussed more here. Further study on the cylindrical coordinates is expected to fulfill the numerical methods in a more realistic physical scheme for the kinematic model.

With the previous grid dependence test and the above validation, it can be briefly concluded at present that under the Cartesian form transition, Method 1 (the second-order accurate forward or backward difference scheme) is more preferable than Method 2 (the central difference scheme) in the perspective of grid dependence. But more generally, Method 1 and Method 2 could both give satisfied results in PBR application. Therefore, both of the boundary methods can be recommended as appropriate numerical solutions for any PBR geometry when their own inherent defects are well treated such as the grid dependence.

In addition to the experimental results, simulated velocity profiles derived by kinematic model, although through different numerical solution, are also given in [5]. The different diffusion lengths B in the model are best fitted from corresponding experimental profiles (see legends in Figure 4). In the original model, B is constant in a determined geometry and depends on the pebble property [11,12], and the value of B was thought to be typically in the range of one to three times of the granule diameter in silos in the early studies. However, it is found that a single fitting B does not suffice to reproduce the entire flow field [14,15]. Later studies found that B is also related with the height and the geometry angle. This could be also concluded with the limited data given by [5], in which Figure 4 certifies clearly that B increases with the height in a given geometry and depends on the slope angle. Nowadays, the imprecise prediction of kinematic model is still a common concern in simulations and experiments. Several researches focused on the velocity profiles in silos using kinematic model as well as experiments [14,16], in which they give similar conclusions and even nonlinear functions on the height dependence of B value. However, there are few investigating the B value in a hopper (PBR) geometry, and the experiments-generated functions in [14,16] based on the silo geometries could not be directly applied to give a certain B value in PBR geometry. Therefore, later in this paper, we are more focused on the B effects on the velocity profiles prediction and its further impacts on the core physics analysis in PBR applications, which will be discussed later in Section 4.

Further work has been under plan to give the functional relation between B and the geometrical parameters in HTR geometry and to improve the accuracy of the kinematic model. Moreover, there are some other advanced continuum-based theories/models [17,18] proposed to describe the stress/strain of the granular flow and may give a better description of the general field. It is worth trying to obtain and compare the mean flow profile of the kinematic, constitutive and DEM methods, which could also help investigating the microscopic justification of B.

4. Applications of pebble velocity profiles in PBR

The subsequent purpose of this research on pebble flow is to generate the burnup distribution of fuel pebbles. The fuel pebble burnup is thought to be closely relevant to the pebble velocity profile and the nonuniform distribution of neutron flux. The time-dependent analysis of burnup can be performed by using the batch-tracking method [19]. In this method, the core is first divided into several axial flow channels by mean pebble residence time of each channel, which is the average time a pebble takes to pass the reactor channel from top to bottom. Then, with different fluxes and residence times given in different channels, Monte Carlo codes for particle transport and the burnup calculation are carried out to track the fuel pebble burnup. In this section, we investigate issues of pebble residence time and channel scheme, which rely on pebble flow velocity profile as an

initial and essential input and eventually contribute to the pebble burnup assay.

Although the geometrical parameters of the referenced geometry in the validation section are not exactly the same as the HTR-PM geometry, the geometry construction in the validation part is almost the same as HTR geometry. Therefore, the two numerical methods validated in the reference geometry could be directly used for generating the velocity profiles in HTR-PM geometry without any further validation tests. The realistic HTR-PM geometry consists of 6-cm-diameter spherical pebbles, an upper cylindrical container approximately 1150 cm high and 300 cm across, a conical funnel region with a slope angled at 30°, and an exit pipe with a radius of 25 cm and a height of 650 cm. Let $z = 0$ be at the bottom orifice, and the initial velocity be 6.25×10^{-3} cm/s, which is estimated from the realistic drainage of approximately 6000 pebbles per day.

4.1. Pebble residence time

Setting to predict the pebble residence time, a previous pebble streamline depiction work is required. The streamlines could be computed by the integration of the velocity profile. First, both the vertical and horizontal velocity data could be bilinear-interpolated to construct a more detailed picture of the velocity field. Then, a particular streamline could be solved by numerically integrating $dX/dt = V(X(t))$, where $X(t) = (r(t), z(t))$ is the position in the streamline at a certain time step; $V(X(t))$ is the vector velocity (composed by the vertical and horizontal) at $X(t)$.

Figure 5 shows the streamlines of pebble flow in HTR-PM. It also indicates the overall shape of pebble flow in PBR, quite consistent with the standard engineering picture of silo drainage [3], with uniform plug flow in the upper cylindrical region, a transition from plug flow to nonuniform converging flow in the cone region and plug flow again in the exit pipe. This rapid transition from plug flow to converging flow could also be explained by the velocity profiles in the core (Figure 6).

We find that the generated horizontal and vertical velocity profiles (u and V) behave differently at different heights near boundary as shown in Figure 6. The u profile shows a small rise and fall over α, and it is much smaller than V profile in most radial range, especially the upper cylindrical region u is smaller than V over the entire range of α (dash-dotted line). However, in the transition section of the funnel and the upper cylinder, u profile coincides with V profile near boundary (solid line), and in funnel region it turns to be slightly higher than V around boundary (dashed line). Thus, the higher u causes bigger horizontal movement around boundary, which could well explain the flow regime transfer in the transition region.

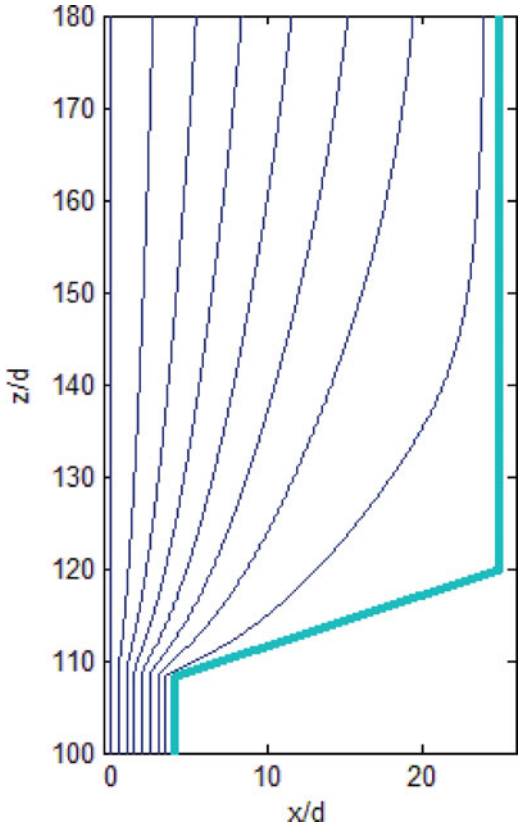

Figure 5. The brief depiction of pebble streamlines in HTR-PM ($B = 3d$) (the outermost line is physical core boundary).

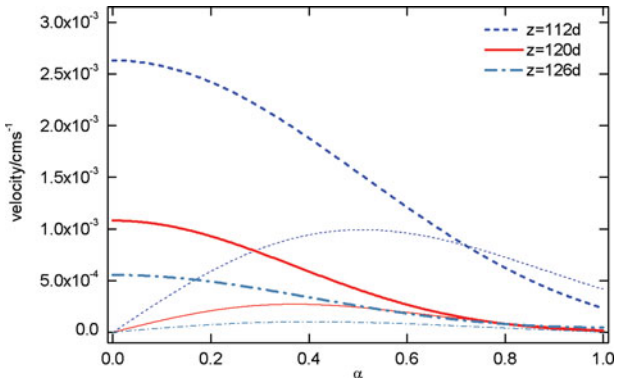

Figure 6. Vertical (heavy lines) and horizontal (thin lines) velocity profiles over α at some certain heights in reactor core when $B = 3d$.

Because of the uniform plug-flow velocity which 'diffuses' from the initial velocity given at the bottom of the pipe, the pebble residence times of different streamlines in lower exit pipe are almost the same and have little impact on reactor physics analysis. Therefore, we approximate the pebble residence time T as the time of pebble to travel along streamline only in the upper cylinder and funnel, stated as Equation (17),

$$T = \sum_{i=L\ldots M} dz/V_j^i, \tag{17}$$

where dz is the grid spacing in the z direction, L is the starting point of the funnel region. The solid line in Figure 7 shows a general picture of residence times of

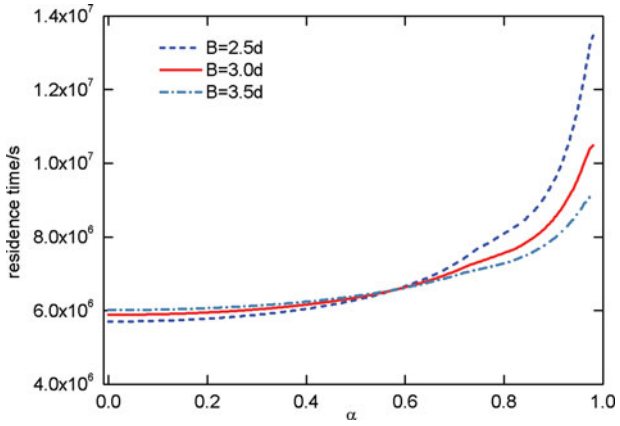

Figure 7. The variance of pebble residence times along streamlines over the range of α for different values of diffusion length B.

streamlines over the range of α when diffusion length $B = 3d$, displaying a steady phase in the center and a rapid growth around boundary. The mean residence time of streamlines is generated as 78.31 days, and it is close to the corresponding pebble residence time in HTR-PM, which is estimated at approximately 70 days.

In Section 2, the diffusion length B has been confirmed as inconstant in a certain geometry, and predictions have been made that the uncertainty would consequently impact the core physics analysis in PBR applications. Here, we perform this impact on pebble residence times with comparisons of results derived from different B values, as shown in Figure 7. It reveals that the residence times in central core region, which is approximately in the range of $0 < \alpha < 0.6$, increase slightly with the diffusion length, whereas for streamlines in the boundary region, $\alpha > 0.6$, the residence times decrease fairly substantially with B, especially near the boundary. We calculate the pebble residence times in the upper cylinder and lower funnel, respectively; analysis shows that residence times in the upper cylinder and the lower funnel both increase mildly with B in the central core region and decrease with B in the boundary region. A reasonable implication of ups and downs of residence times with B in the upper cylinder and lower funnel is that diffusion length influences velocity differently in different radial regions. This can be verified by simulation results that an increased B derives higher vertical velocity in the central core region and lower vertical velocity in the boundary region, and thus an increased B would generate a more gentle and uniform vertical velocity field. In general, pebble residence time can be influenced by the undetermined B, and this will lead to changes in channel scheme which will be discussed in Section 4.2.

4.2. Channel scheme of core region

Since the pebbles are not in a flow of uniform speed, dividing the container into channels which are equally spaced in radius is unsatisfactory [8]. Therefore, most of the pebble flow models have been divided into a certain number of channels with unfixed width according to the flow velocity distribution. The THTR reactor core was divided into nine axial channels in pebble flow model [20]. Kim et al. tried to divide the annular core region of PBMR into six channels with respect to an angular direction [21]. The Jüelich Research Center used flow models with reactor core divided into 17 axial channels in the VSOP code, which has been recognized as the standard for most PBR analysis [22].

Previous researches on HTR-PM in China generated a channel scheme, in which the half-size core is divided into eight axial channels, and derived a mean residence time ratio (the mean residence time of each channel normalized by the mean residence time of the first central channel) as: 1:1:1:1:1.125:1.125:1.125:1.5. According to this ratio, we propose and compare two different axial eight-channel schemes.

4.2.1. Channel scheme 1

Channel scheme 1 starts from the principle that the fluctuations in residence times of streamlines within each channel should be within a certain range. Thus, the scheme confirms that the times along any streamline within the channel do not vary too much. In the previous research on HTR-PM, the eight channels can be basically grouped into three primary channels according to the mean residence time ratio: the first four channels, the subsequent three channels and the last channel. On the basis of this scheme, we propose an identical but advanced channel scheme. Since the residence times of streamlines keep stable in central region while increase much near boundary (already shown in Figure 7), the streamlines are first divided into four primary channels, with one more channel set in the boundary region compared to the previous research. The division of the four primary channels requires that the relative standard deviation (RSD) of the streamline residence times within the primary channel should be basically the same. Therefore, the residence time RSD for the four primary channels are derived as approximately 6.5% as B equals to $2.5d$. Then, the first and the second primary channels are, respectively, divided into four and two sub-channels. It is also required that the RSD of the streamline residence times of the sub-channels in a primary channel should be basically the same. Hence, the residence time RSD of the sub-channels in the first primary channel is obtained as about 1.6%, while the residence time RSD of the sub-channels in the second primary channel is around 3.4%. The third and the fourth primary channels would not be divided into sub-channels due to their fairly narrow radial range (see Table 1). Thus, the half-core has been divided into eight channels.

As the impacts of inconstant B on pebble residence time have been analyzed in Section 4.1, its subsequent

Table 1. Channel scheme 1 of a half-size HTR-PM core.

		Ch.							
B		1	2	3	4	5	6	7	8
2.5d	R/cm	0.00–57.75	57.75–78.38	78.38–91.88	91.88–101.63	101.63–117.38	117.38–131.25	131.25–141.00	141.00–147.00
	$\overline{T_i}$/day	67.22	71.52	75.63	79.95	87.22	97.12	113.94	142.55
	R^*	1.00	1.06	1.13	1.19	1.30	1.44	1.69	2.12
3.0d	R/cm	0.00–54.00	54.00–73.88	73.88–87.38	87.38–97.50	97.50–114.75	114.75–129.00	129.00–140.25	140.25–147.00
	$\overline{T_i}$/day	68.98	71.94	74.70	77.56	82.39	88.65	98.58	114.59
	R^*	1.00	1.04	1.08	1.12	1.19	1.29	1.43	1.66
3.5d	R/cm	0.00–51.38	51.38–70.50	70.50–83.63	83.63–93.75	93.75–109.50	109.50–126.38	126.38–139.50	139.50–147.00
	$\overline{T_i}$/day	70.25	72.45	74.44	76.46	79.60	83.98	90.98	101.63
	R^*	1.00	1.03	1.06	1.09	1.13	1.20	1.30	1.45

R is the radius range of each channel in the upper cylinder region.
$\overline{T_i}$ is the mean residence time of each channel.
R^* is the general mean residence time ratio of each channel.

influences on channel scheme are focused as well. We propose three similar eight-channel schemes making use of the obtained residence time when B is varied to 2.5d, 3d and 3.5d (see Table 1). Except for the case of $B =$ 2.5d mentioned above, we also derive the residence time RSD for primary channel as B equals to 3.0d and 3.5d, which are 4.5% and 3.0%. Table 1 gives the acquired radius range of each channel in the upper cylindrical region, which also confirms that the channels are not equally spaced given the nonuniform velocity profiles.

Table 1 also shows the influence of B on channel scheme and corresponding mean residence time of each channel. An increased B would result in a more inward-concentrated channel scheme with different radius range. The mean residence time of each channel decreases with B except for the first two channels, inducing a decreased general mean residence time ratio. In general, an increased B would give a more gentle and uniform picture of the mean residence time over the radius range; the residence time RSD values indicate that this eight-channel scheme is more appropriate and accurate for a big B case.

4.2.2. *Channel scheme 2*

Channel scheme 2 is proposed on the principle that each axial channel should be of equal volume, which has been used already in previous research. We first calculate the radius range of each equal-volume channel in the eight-channel scheme, and then generate the corresponding mean residence times of each channel with B being 2.5d, 3d and 3.5d, respectively (Table 2).

Table 2 shows that B has an impact on the mean residence time of each channel, even though the channel scheme is determined with fixed radius range. Similarly, with the scheme 1, an increased B gives a longer mean residence time in the central region and a shorter mean residence time in the boundary region, eventually generating a more uniform mean residence time picture.

Although radius of channels in scheme 1 would vary with B while the radius range in scheme 2 is fixed and constant, the mean residence time of each channel in both channel schemes would be influenced by B. In general, scheme 1 gives higher mean residence time ratio than scheme 2.

Although B is still undetermined for its complex dependence on pebble property and core geometry,

Table 2. Channel scheme 2 of a half-size HTR-PM core.

		Ch.							
B		1	2	3	4	5	6	7	8
	R/cm	0.00–51.75	51.75–73.50	73.50–90.00	90.00–103.88	103.88–116.25	116.25–127.50	127.50–137.63	137.63–147.00
2.5d	$\overline{T_i}$/day	66.98	70.56	74.67	80.11	87.58	95.13	106.61	135.19
	R^*	1.00	1.05	1.11	1.20	1.31	1.42	1.59	2.01
3.0d	$\overline{T_i}$/day	68.91	71.78	74.96	78.98	83.94	88.56	96.10	111.75
	R^*	1.00	1.04	1.09	1.15	1.22	1.29	1.39	1.62
3.5d	$\overline{T_i}$/day	70.26	72.63	75.21	78.34	81.89	85.12	90.56	100.43
	R^*	1.00	1.03	1.07	1.12	1.17	1.21	1.29	1.43

R is the radius range of each channel in the upper cylindrical region.
$\overline{T_i}$ is the mean residence time of each channel.
R^* is the general mean residence time ratio of each channel.

the B influences on pebble residence time and channel scheme are concerned in this section. This impact can be eventually attributed to the conclusion proposed in Section 4.1 that vertical velocity increases with B in the central region but decreases with B in the boundary region.

5. Conclusions and discussion

This paper investigates numerical solutions for the kinematic model of pebble flow velocity profiles in PBR geometry. The method is based on a previously proposed transformed Cartesian coordinates and uses the implicit Crank–Nicholson integration scheme with two different treatments of the boundary conditions. One is the second-order accurate forward or backward difference scheme (Method 1) which is our first original attempt; another is the referenced central difference scheme (Method 2). Eventually, the matrix equation generated by the above discretized equations is solved by the chasing method. The grid dependence of the velocity profiles with the two methods is tested. The simulated velocity profiles are compared and validated by experimental results from the reference. It can be briefly concluded at present that under the Cartesian form transition, Method 1 is more preferable than Method 2 in the perspective of grid dependence. But more generally, Method 1 and Method 2 could both give satisfied results in PBR application. Therefore, both of the boundary methods can be recommended as appropriate numerical solutions for any PBR geometry.

It is noticed that the introduced Cartesian coordinates allow to solve the problem over the range $0 < \alpha < 1$ independent of R, being a function of z, which would otherwise further complicate the mesh scheme in the non-rectangular simulation domain. Besides the shock-like boundary, velocity instabilities for steep cone geometry in cylindrical coordinates should be further studied, because cylindrical form equation matches physical geometry better and may be easily applied in reactor physics or thermal hydraulics. Besides, although the recommended methods give preferable agreements with the referenced experimental results, the agreements of relative vertical velocity do not suffice to validate the absolute value of vertical velocity in reality, hence explicit experiments are expected for a better validation.

Two pebble burnup-related issues, which are the pebble residence time prediction and the channel scheme in the realistic HTR-PM geometry core, are investigated with the velocity profiles. The pebble residence times along streamlines are calculated out with the streamlines depicted by the integration of the velocity profile. By reference to the mean residence time ratio in previous research, two different axial eight-channel schemes, which are respectively based on the similar streamline residence time principle and the equal-volume channel principle, are proposed and compared. Furthermore, due to the complex evaluation of diffusion length B in reactor core, the impacts of varied B on pebble residence time and channel scheme are investigated. It is concluded that an increased B would give a more gentle and uniform picture of mean residence time in both schemes, and the eight-channel scheme 1 is more accurate and appropriate for a big B case. This B impact could be eventually attributed to the fact that vertical velocity increases with B in the central core region but decreases with B in the boundary region. The two channel schemes give identical general mean residence time ratio, but they differ in basic principles and final results, and no conclusions on the scheme preference are made. Moreover, both channel schemes are proposed by previous experience and will be adjusted to be more appropriate and complete according to subsequent burnup calculation.

In spite of the advantages of mathematical simplicity and completeness, however, the kinematic model with the only fixed parameter for certain geometry cannot exactly simulate some regions. It is found that the diffusion length not only depends on the pebble property, but also increases with the height and varies with the slope angle. As the solution for precisely determining B is still lacking, B-induced inaccuracy can impact core physics analysis in PBR applications as verified in this paper. Future work on the functional relation between B and the geometrical parameters is expected to better describe the general field with our future DEM results on HTR-PM. Studies on other advanced continuum-based theories/models are planned to help investigate the microscopic justification of B as well.

Acknowledgments

This project is supported by Beijing Natural Science Foundation [grant number 1154010] and Nuclear Energy Development Project jointly.

Disclosure statement

No potential conflict of interest was reported by the authors.

References

[1] DoE. A technology roadmap for generation IV nuclear energy systems. San Diego, CA: The Generation IV International Forum; 2002. p. 9.
[2] Zhang Z, Wu Z, Sun Y, et al. Design aspects of the Chinese modular high-temperature gas-cooled reactor HTR-PM. Nucl Eng Des. 2006;236:485–490.
[3] Rycroft CH, Grest GS, Landry JW, et al. Analysis of granular flow in a pebble-bed nuclear reactor. Phys Rev E. 2006;74:021306.
[4] Tang Y, Zhang L, Guo Q, et al. A proposed model to describe the relationship between online burnup assay and economy and safety of pebble bed reactor, 24th International Conference on Nuclear Engineering, Charlotte, North Carolina; 2016.

[5] Choi J, Kudrolli A, Bazant MZ. Velocity profile of granular flows inside silos and hoppers. J Phys Condens Matter. 2005;17:S2533.
[6] Goodling J, Vachon R, Stelpflug W, et al. Radial porosity distribution in cylindrical beds packed with spheres. Powder Technol. 1983;35:23–29.
[7] Rycroft CH, Orpe AV, Kudrolli A. Physical test of a particle simulation model in a sheared granular system. Phys Rev E. 2009;80:031305.
[8] Kim SH, Kim H-C, Kim JK, et al. A study on evaluation of pebble flow velocity with modification of the kinematic model for pebble bed reactor. Ann Nucl Eng. 2013;55:322–330.
[9] Nedderman R, Tüzün U. A kinematic model for the flow of granular materials. Powder Technol. 1979;22:243–253.
[10] Li Y, Ji W. Acceleration of coupled granular flow and fluid flow simulations in pebble bed energy systems. Nucl Eng Des. 2013;258:275–283.
[11] Mullins W. Experimental evidence for the stochastic theory of particle flow under gravity. Powder Technol. 1974;9:29–37.
[12] Tüzün U, Nedderman R. Experimental evidence supporting kinematic modelling of the flow of granular media in the absence of air drag. Powder Technol. 1979;24:257–266.
[13] Mathews JH, Fink KD. Numerical methods using MATLAB. 4th ed. Upper Saddle River, NJ: Pearson; 2010. p. 109.
[14] Medina A, Cordova J, Luna E, et al. Velocity field measurements in granular gravity flow in a near 2D silo. Phys Lett A. 1998;250:111–116.
[15] Nedderman RM. Statics and kinematics of granular materials. 1th ed. New York, NY: Cambridge University Press; 1992.
[16] Sielamowicz I, Czech M, Kowalewski TA. Empirical description of granular flow inside a model silo with vertical walls. Biosyst Eng. 2011;108:334–344.
[17] Jop P, Forterre Y, Pouliquen O. A constitutive law for dense granular flows. Nature. 2006;441:727–730.
[18] Forterre Y, Pouliquen O. Flows of dense granular media. Annu Rev Fluid Mech. 2008;40:1–24.
[19] Kim H-C, Kim J, Kim S, et al. Monte Carlo benchmark calculations for 400MW T H PBMR core. 13th ICENES; 2007; Istanbul.
[20] Zhong W, Jing X, Luo J, et al. A simulation of the pebble bed reactor core in HTR. Chinese J Nucl Sci Eng. 1993;13:110–118.
[21] Kim HC, Kim SH, Kim JK, et al. Monte Carlo burn-up calculation of the PBMR core with pebble flow velocity. Korean Nuclear Society Autumn Meeting; 2010; Jeju, Korea.
[22] Kadak AC, Bazant MZ. Pebble flow experiments for pebble bed reactors. 2nd International Topical Meeting on High Temperature Reactor Technology, Beijing, China; 2014.